



# Numerical modeling of three-phase flow through a Venturi meter using the LSSVM algorithm

Omid Khayat and Hossein Afarideh\*

Energy Engineering and Physics Department, Amirkabir University of Technology, 424 Hafez Ave., Tehran, Iran

---

**Article info:**

Type: Research  
Received: 24/05/2018  
Revised: 03/04/2019  
Accepted: 12/04/2019  
Online: 15/04/2019

**Keywords:**

Measurement,  
Three phase flow,  
Computational fluid  
dynamics,  
Venturi meter,  
LSSVM algorithm.

**Abstract**

One of the challenging problems in the oil and gas industry is accurate and reliable multiphase flow rate measurement in a three-phase flow. The application of methods with minimized uncertainty is required in the industry. Previously developed correlations for two-phase flow are complex and not capable of three-phase flow. Hence phase behavior identification in different conditions of designing and modeling of three-phase flow is important. Numerous laboratory and theoretical studies have been done to describe the Venturi multiphase flow meter in both horizontal and vertical flow. However, it is not possible to select the measurement devices for all similar conditions. In this study, a new venturi model is developed to implement in Simulink/Matlab for predicting the mass flow rate of gas, water, and oil. This model is simple and semi-linear. Several classified configurations of three-phase flow are simulated using computational fluid dynamics analysis to get hydrodynamics parameters of the flows to use as inputs of the model. The obtained data is used as a test and train data in the least squares support vector machine (LSSVM) algorithm. The pressure drop and mass flow rate of gas, oil, and water are calculated with the LSSVM method. Two tuning parameters of LSSVM, namely  $\gamma$  and  $\sigma^2$ , are obtained as 1150954 and 0.4384, 53.9199 and 0.18163, 8.8714 and 0.14424, and 1003913.2214 and 0.74742 for the pressure drop, the mass flow rate of oil, gas mass flow rate, and the water mass flow rate, respectively. Developed models are found to have an average relative error of 5.81%, 6.31%, and 2.58% for gas, oil, and water, respectively.

## 1. Introduction

Multiphase flow occurs in many industries including food, pharmaceutical, nuclear, chemical, and petroleum. Anticipating a three-phase flow pressure gradient is an important step in the design of such industrial processes. Yeung et al. [1] mentioned that multiphase flow measurement is significantly more complex and inaccurate than measuring a single phase one,

and despite significant progress in the recent years in this area, using methods with minimized uncertainty is required in the industry. Falcone et al. [2] emphasized that the most accurate technique for measurement of multiphase flow is separating the mixture and utilizing conventional devices for measuring single-phase flow. However, the cost, practicability, and transportation problems are limitations for this method. Brill [3] stated that multiphase

---

\*Corresponding author  
email address: hafarideh@aut.ac.ir

modeling approaches for finding the best equation for measuring mass flow rate include experimental, theoretical, and simulation techniques. So far, many experiments have been done for measuring two-phase flow properties using different experimental devices like pressure devices associated with other types of meters, like void fraction sensors and conductance probes. At Pisa University in 1989, a research project initiated on the Venturi nozzle application for industrial multiphase mass flow rate measurements. Azzopardi and Govan [4] and Pulley [5] generated a mechanistic model for the flow through a Venturi nozzle by assuming conditions of annular flow and investigating the dispersed droplet flow effect on the pressure drop. Murdock [6] studied the overall case of two-phase flow in an orifice plate meter which was not limited to wet gas flows only. Lin [7] extended a model based upon separating flow model (for general stratified two-phase flow), in which the mass flow quality must be known. Smith and Leang [8] worked on a model that takes into account the presence of liquid by defining a new factor called 'blockage factor (BF)' which can be applied for Venturi meters and orifice plates. De Leeuw [9] developed a correlation for anticipating the effect of the liquid phase presence on Venturi meter reading, which is a modified form of Chisholm [10] correlation. Steven [11] found that de Leeuw correlation was not reliable for NEL wet gas loop, so he developed a new correlation by independent data from the NEL wet gas loop, giving a well fit for a 6 inch Venturi and 0.55 diameter ratio geometry. These correlations are based on the quality of mass flow.

Tukimin et al. [12] analyzed the flow through the venturi tube and its discharge coefficient by computational fluid dynamics (CFD) for accurate administration of the venturi tube discharge coefficient, and they achieved a reasonable match with experimental results. Furthermore, measurements of mass flow rate in gas-liquid flows using a venturi or orifice plate joined to a void fraction sensor have been done by Oliveira et al. [13]. He and Bai [14] developed a new correlation for measurement of wet gas flow rate with a Venturi meter based on a two-phase mass flow coefficient. Xu et al. [15]

investigated differential pressure signal dynamic fluctuation of Venturi meter for wet gas metering, and Moura and Marvillet [16] used Venturi and void fraction meters for measuring two-phase mass flow rate and quality. Gupta et al. [17] explored the two-phase flow of air-water through a venturi at ambient pressure and temperature to find a relationship between void fraction and pressure drop in a two-phase fluid flow. Stenmark [18] conducted a multiphase simulation of air-water two-phase flow in T-junction to find the proper models with consideration of experimental data. They concluded that the Euler-Euler modeling approach has the best compatibility with experimental data in the prediction of volume fraction distribution. Kharoua et al. [19] modeled a three-phase flow in a horizontal separator using the Eulerian-Eulerian approach. They used Population Balance Model for the size distribution of the dispersed phase and concluded that the coarse size distribution at inlet improves the performance of the separators. Multiphase flow in venturi and orifice was distinguished theoretically and experimentally by Silvao et al. [20], Murdock [6], Collins and Gacesa [21], ling et al. [20, 22], and Zhang et al. [23]. They presented different correlations based on the specific conditions of flow. These correlations demonstrate the relationship between pressure drop, flow quality, and mass flow rate. Meng et al. [24] proposed a method for the characterization of air-water two-phase by means of Venturi meter and an electrical resistance tomography sensor (ERT). In that method, the flow pattern information was involved in the measurement process using the ERT sensor, and the effect of flow pattern in the calculation is minimized. Simulation techniques in recent years for multiphase flow metering were studied by Fiebach et al. [25]. They simulated two-phase flow through a vertically mounted venturi flow meter in large pipes to find flow patterns. Frank [26] used a numerical method to investigate 3-dimensional two-phase flow in horizontal pipelines. All of the above methods were used for two-phase flow and have limitations for being used at a three-phase one. So, there is an increasing need for finding

suitable techniques for three-phase flow measurements.

In this study, a pre-processing application tool is utilized to construct the geometry and mesh network of the model. Also, required simulations are selected based on available variables like properties of three phases and hydrodynamic parameters. So, more than 80 simulations are considered. Then, these simulations data are gathered and supported vector algorithm to train and test the model. The goal of this study is to find a mass flow rate in water-oil-gas three-phase flow, and consequently to investigate the effects of variable parameters on the flow rate through a model that is based on simulation study and modeling of venturi meter.

## 2. Problem definition and modeling

### 2.1. Multiphase Venturi meter

Among the several velocity measurement techniques, venturi flow meters with differential pressure transmitters are still broadly utilized because of their robustness, reliability, simplicity, and ease of installation. In some applications, this flow meter is also used to characterize the direction of flow and flow regime. Computation of individual phase parameters (velocities, phase interactions, and phase fraction) from measured variables (pressure drop across the venturi and flow parameters of inlet and outlet) needs comprehensive knowledge of the multiphase flow behavior within the measurement device. The detection of flow regime and connection between the flow rate, void fraction, quality, and measured differential pressure is of fundamental importance.

### 2.2. Numerical modeling

CFD techniques have become standard in numerous aspects of engineering including solid, gas, and liquid transportation [27, 28]. Numerical simulations are utilized in the design phase to select among different ideas and in the production phase to analyze performance. Industrial applications of CFD need great flexibility in the procedure of grid-generation for complex configurations, short turn-around

time, and easy to use environments. Some commercial packages are accessible for the CFD industrial applications. These packages are typically integrated systems which consist of a flow solver, mesh generator, and a visualization tool. Often the numerical methods adopted in these CFD programs are well-accepted algorithms published in the open literature and selection of one technique with respect to others is usually based on robustness and reliability. First, in this study, a pre-processing application (GAMBIT) is utilized to create the model geometry. Boundaries of the model (walls, inlets, and outlets) are also identified in this step. The CFD Solver FLUENT produces the data of the flow field at each mesh point after solving the proper governing equations. Eulerian multiphase model is used to solve the momentum and mass equations which are briefly described below. CFD-Post as a data processor is used to create line plots and contours of flow variables.

In the Eulerian multiphase model, phases are treated as interpenetrating continua and averaging techniques are employed to develop effective conservation equations (mass, momentum, and energy) of each phase. In the simulations, water is considered as the continuous phase. On the other hand, oil and gas are discontinuous phases (as droplets and bubbles with constant diameter). These assumptions are the main approximation of the Eulerian-Eulerian approach. Eulerian multiphase model applications include particle suspension, bubble columns, risers, and rotary beds [29]. Conservation equations are shown below (Manninen et al. [30]):

Continuity:

$$\frac{\partial(\alpha_q \rho_q)}{\partial t} + \nabla \cdot (\alpha_q \rho_q u_q) = \sum_{p=1}^n \dot{m}_{pq} \quad (1)$$

Momentum for q<sup>th</sup> phase:

$$\frac{\partial(\alpha_q \rho_q u_q)}{\partial t} + \nabla \cdot (\alpha_q \rho_q u_q u_q) = -\alpha_q \nabla P + \alpha_q \rho_q g + \nabla \cdot \tau_q + \sum_{p=1}^n (R_{pq} + \dot{m}_{pq} u_q) + \alpha_q \rho_q (F_{lift,q} + F_{vm,q}) \quad (2)$$

The inter-phase exchange forces are expressed as:

$$R_{pq} = K_{pq}(u_p - u_q) \quad (3)$$

The lift force is expressed as follows:

$$F_{lift,q} = -0.5\alpha_p\rho_q(u_q - u_p) \times (\nabla \times u_q) \quad (4)$$

The virtual mass force is given by:

$$F_{vm,q} = 0.5\alpha_p\rho_q \left( \frac{d_q u_q}{dt} - \frac{d_p u_p}{dt} \right) \quad (5)$$

To simulate the fluid flow, a turbulence model is implemented, known as the k-ε turbulence model, developed by Launder and Spalding [31], as described by Versteeg and Malalasekera [32] which adds two partial differential equations to the present system of equations as follows:

$$\frac{\partial k}{\partial t} + v_i \frac{\partial k}{\partial x_i} = \frac{\partial}{\partial x_i} \left( \frac{v_t}{\sigma_k} \frac{\partial k}{\partial x_i} \right) + v_t \left( \frac{\partial v_i}{\partial x_j} + \frac{\partial v_j}{\partial x_i} \right) \frac{\partial v_i}{\partial x_j} - \varepsilon \quad (6)$$

$$\frac{\partial \varepsilon}{\partial t} + v_i \frac{\partial \varepsilon}{\partial x_i} = \frac{\partial}{\partial x_i} \left( \frac{v_t}{\sigma_\varepsilon} \frac{\partial \varepsilon}{\partial x_i} \right) + C_{1\varepsilon} \frac{\varepsilon}{k} v_t \left( \frac{\partial v_i}{\partial x_j} + \frac{\partial v_j}{\partial x_i} \right) \frac{\partial v_i}{\partial x_j} - C_{2\varepsilon} \frac{\varepsilon^2}{k} \quad (7)$$

In this study, unstructured tetrahedral hybrid cells are used to generate a mesh on the entire flow domain. Grid independence tests are carried out by progressively increasing the number of cells for the simulations. The tests are done for computational grids of 100000 to 700000 cells (Fig. 1). Finally, the approximately 310000 cells of the computational grid are chosen here due to its perfect prediction and economic computation. The structure of the generated mesh for Venturi meter is shown in Fig. 2. All the simulations are conducted in a steady-state condition, and the phases are considered incompressible.

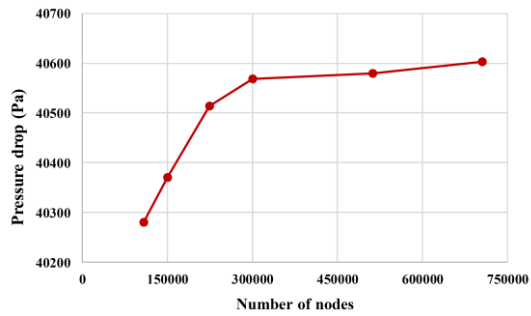


Fig. 1. Mesh independency.

For validation of the CFD results, simulation of single-phase flow is compared with the work of Sanghani and Jayani [33] and is shown in Table 1. It can be seen that the value of pressure drop obtained through simulation is within 93% of the confidence interval as well as it is slightly more than the value of pressure drop obtained by the work of Sanghani and Jayani [33].

### 2.3. Data analysis

The data used for this work is obtained from CFD calculations of more than 80 cases. Several researchers used the CFD method to study and evaluate the venturi meter in industrial applications. Perez et al. [34] presented 3D numerical simulations of liquid-gas flows in the pertinent segments of the multiphase loop at Neat-Petrobras for calibration of an ultrasonic multiphase flow meter. The flow pattern prediction of their simulation showed good agreement with Baker flow pattern map. Michele and Hempel [35] developed modeling calculations using computational fluid dynamics. Their results showed that CFD modeling approaches can gather important information about flow structure and dispersed phase distribution, and then experimental investigation verified their CFD calculation. Ekambara et al. [36] demonstrated phase distribution of co-current and air-water bubbly flow in a horizontal pipeline.

Table 1. Comparison between results of simulation and Sanghani and Jayani [32] work.

Parameters				Pressure drop through venturi meter (Pa)	
Convergent cone angle $\theta_c$	Divergent cone angle $\theta_d$	Throat length ( $l, cm$ )	Beta ratio	Present work	Sanghani and Jayani [33]
17	7	0.007	0.75	40599.4	37757.7

They obtained a worthy quantitative agreement with the experimental data with two different models ( $k-\varepsilon$  with constant bubble size and  $k-\varepsilon$  with population balance model). Therefore, the present investigation on fluid flow is carried out using CFD calculation in FLUENT software. The aim is to develop models for the mass flow rate of gas, water, and oil in multiphase flow through Venturi. In this work, five different geometries are investigated. Schematic of the venturi with different throat-pipe diameter ratio is illustrated Fig. 2.

The domain of flow includes a pipe of 28mm internal diameter having venturi meter fitted at a distance of 100 mm from the inlet. Following parameters range is considered in this model:

$$\begin{aligned} 500 \left( \text{Kg}/\text{m}^3 \right) < \rho_o < 950 \left( \text{Kg}/\text{m}^3 \right) \\ 0.05 \left( \text{Kg}/\text{m}^3 \right) < \rho_g < 4 \left( \text{Kg}/\text{m}^3 \right) \\ 0.2 < \varphi_o < 0.7 \\ 0.1 < \varphi_g < 0.6 \\ 0.25 < \beta < 0.8 \end{aligned}$$

#### 2.4. LSSVM algorithm

The support vector machine (SVM) is a novel machine-learning algorithm having outstanding characteristics. The least square support vector machine (LSSVM) algorithm is an improved algorithm of SVM. Baghban et al. [37] described the LSSVM algorithm. Standard SVM was solved by Suykens et al. [38] using quadratic programming techniques.

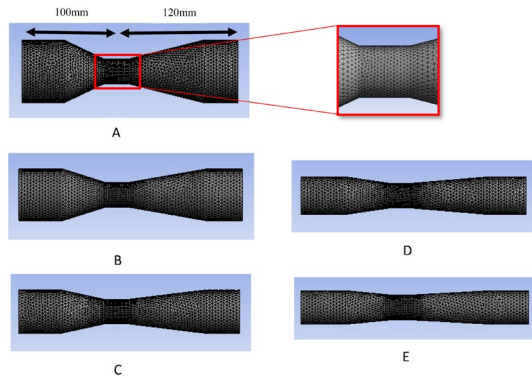


**Fig. 2.** Schematic of the venturi meters used in CFD calculation; (A)  $\beta = 0.4$ , (B)  $\beta = 0.4875$ , (C)  $\beta = 0.575$ , (D)  $\beta = 0.6625$ , (E)  $\beta = 0.75$ .

In order to make the algorithm applicable for non-linearly separable datasets and also capable of less sensitive to outliers, the present optimization is reformulated as follows:

$$\frac{1}{2} \|w\|^T w + C \sum_{i=1}^N \xi_i + \xi_i^* \quad (8)$$

Subject to:

$$\begin{cases} (y_i - (w, \phi(x_i)) - b) \leq \varepsilon + \xi_i \\ (w, \phi(x_i)) + b - y_i \leq \varepsilon + \xi_i^* \\ \xi_i, \xi_i^* \geq 0 \end{cases} \quad (9)$$

The Lagrangian can be formed:

$$\begin{aligned} L_{svm} &= \frac{1}{2} \|w\|^2 + C \sum_{i=1}^l (\xi_i + \xi_i^*) \\ &\quad - \sum_{i=1}^l (\eta_i \xi_i + \eta_i^* \xi_i^*) \\ &\quad - \sum_{i=1}^l \alpha_i (\varepsilon + \xi_i - y_i + (w, x_i) + b) \\ &\quad - \sum_{i=1}^l \alpha_i^* (\varepsilon + \xi_i^* + y_i - (w, x_i) - b) \end{aligned} \quad (10)$$

where  $L$  is the Lagrangian and  $\eta_i, \eta_i^*, \alpha_i, \alpha_i^*$  are lagrangian multipliers.

Great computational work for constrained optimization programming is the drawback of SVM. LSSVM is preferred particularly for large scale problems, and resolves the SVM drawback by solving linear equations instead of a quadratic programming problem.

By reducing the empirical risk function in the feature space with a squared loss, the subsequent primal optimization problem can be obtained (Hoerl and Kennard [39]).

$$\min j(w, e)_{w.b.e} = \frac{1}{2} \|w\|^2 + \frac{1}{2} \gamma \sum_{i=1}^N e_i^2 \quad (11)$$

Subject to:

$$y_i = (w, \phi(x_i)) + b + e_i, \quad i = 1, \dots, N \quad (12)$$

The comparative importance of these terms is determined by the positive real constant  $\gamma$ . The above relation is correlated to ridge regression. As shown below, this problem is solved easily by setting the partial derivatives equal to zero:

$$\frac{\partial j(w,e)_{w,b,e}}{\partial(w)} = 0 \quad \text{and} \quad \frac{\partial j(w,e)_{w,b,e}}{\partial(e)} = 0 \quad (13)$$

For solving the optimization problem in the dual space, the following equation can be defined:

$$L_{lssvm} = \frac{1}{2} \|w\|^2 + \frac{1}{2} \gamma \sum_{i=1}^N e_i^2 - \sum_{i=1}^N \alpha_i \{ (w \cdot \phi(x_i)) + b + e_i - y_i \} \quad (14)$$

The solution given by Lagrangian saddle point with Lagrange multipliers  $\alpha_i \in \mathbb{R}$  (are called support vectors) is:

$$\begin{cases} \frac{\partial L_{lssvm}}{\partial w} = 0 \rightarrow w = \sum_{i=1}^N \alpha_i \phi(x_i) \\ \frac{\partial L_{lssvm}}{\partial b} = 0 \rightarrow \sum_{i=1}^N \alpha_i = 0 \\ \frac{\partial L_{lssvm}}{\partial e_i} = 0 \rightarrow \alpha_i = \gamma e_i \quad i = 1, \dots, N \\ \frac{\partial L_{lssvm}}{\partial \alpha_i} = 0 \rightarrow (w \cdot \phi(x_i)) + b + e_i - y_i = 0 \end{cases} \quad (15)$$

Set of linear equations:

$$\begin{bmatrix} I & 0 & 0 & -z^T \\ 0 & 0 & 0 & -y^T \\ 0 & 0 & \gamma I & -I \\ z & y & I & 0 \end{bmatrix} \begin{bmatrix} w \\ b \\ e \\ \alpha \end{bmatrix} = \begin{bmatrix} 0 \\ 0 \\ 0 \\ \vec{1} \end{bmatrix} \quad (16)$$

with

$$\begin{aligned} Z &= [\phi(x_1)^T y_1, \dots, \phi(x_N)^T y_N] \\ Y &= [y_1, \dots, y_N] \\ \vec{1} &= [1, \dots, 1] \\ e &= [e_1, \dots, e_N] \\ \alpha &= [\alpha_1, \dots, \alpha_N] \end{aligned}$$

After elimination of  $w, e$ , the solution yields:

$$\begin{bmatrix} 0 & y^T \\ y & \Omega + \gamma^{-1}I \end{bmatrix} \begin{bmatrix} b \\ \alpha \end{bmatrix} = \begin{bmatrix} 0 \\ \vec{1} \end{bmatrix}$$

where  $\Omega = ZZ^T$  (17)

And Mercer's condition is applied:

$$\Omega_{il} = y_k y_l \phi(x_i) = y_k y_l K(x_i \cdot x_l) \quad (18)$$

Many kernel functions such as linear, polynomial, radial basis function (RBF), and sigmoid are stated. However, the greatest popular kernel functions are RBF (Eq. 15) and polynomial (Eq. 20).

$$K(x_i, x_j) = \begin{cases} x_i \cdot x_l & \text{linear} \\ (\gamma x_i \cdot x_l + C)^d & \text{polynomial} \\ \exp(-\gamma |x_i - x_l|^2) & \text{RBF} \\ \tanh(\gamma x_i \cdot x_l + C) & \text{sigmoid} \end{cases} \quad (19)$$

where:

$$K(X_i \cdot X_l) = \phi(X_i)^T \cdot \phi(X_l) \quad (20)$$

$$K(x_i, x_l) = \exp\left(-\frac{\|x_i - x_l\|^2}{\sigma^2}\right) \quad (21)$$

$$K(x_i, x_l) = \left(1 + \frac{x_k^T x_l}{C}\right)^d \quad (22)$$

where  $\sigma^2$  and  $d$  are the squared variance of the Gaussian function and polynomial degree respectively. As a result, in the LS-SVM case, every data point is a support vector. This is obvious from the condition for optimality:  $\alpha_i = \gamma e_i, i = 1, \dots, n$

### 3. Result and discussion

The relationship between the mass flow rate and the pressure difference measured via a venturi nozzle in the single-phase flow is given by:

$$\Gamma = C \varepsilon A_2 \sqrt{\frac{2 \Delta P \rho_L}{1 - \beta^4}} \quad (23)$$

The compressibility coefficient  $\varepsilon$  is equal to 1 for an incompressible flow. It is less than 1 for a compressible flow. The discharge coefficient  $C$  which is generally obtained by calibration and depends on the geometry of the device is very close to 1.  $\Delta P$  refers to pressure drop through the venturi.  $\beta$  is the diameter ratio of throat-pipe,

and  $\rho$  is fluid density. Most of the national codes (ASME, UNI, DIN) provide  $C=0.995$  in the following range of parameters:

$$50 < D < 250 \text{ mm}$$

$$0.4 < \beta < 0.75$$

$$10^5 < R_e < 10^6$$

Present measurements, which cover a wide range of gas and liquid flow rates, have been tentatively correlated by a semi-empirical equation recommended by Chisholm [10]. Eq. (23) is based on a constant slip ratio between the liquid and the gas phases. Also, Martinelli parameter must be calculated in this model.

The continuity and momentum equations, known as the Navier-Stokes equations, are required to define the state of any flow regime and are normally used for all fluid flows in CFD modeling. Supplementary equations like the energy and turbulence equations, might be required to appropriately define a flow depending on the particular flow nature. Modeling of multiphase flow is very complex, and performing numerical study has associated with limitation in time, computer capacity, uncertainty, etc. The transport equations method executed commonly in CFD programs is the finite volume method (FVM). Two main multiphase models are available: homogeneous and inhomogeneous models. The homogeneous model relates to a VOF model. The inhomogeneous one is based on the Euler method and can be used together with some

subsidiary models to describe dispersed flow, mixtures of continuous fluids, and so on.

In this modeling, the density and volume fraction of water are  $998.2 \text{ Kg/m}^3$  and 0.2, respectively.

The cases of the simulation are classified using design expert® software, V10. The collected data is shown in Table I (Appendix). This design includes 42 non-center points and 1 center point. The response surface method (RSM) is selected to design the experiments. Analyzing the mentioned parameters is shown in Figs. 3-5 which show how the mass flow rate of three phases is affected by density, throat-pipe diameter ratio, and volumetric ratio of each phase. As illustrated in Fig. 3(a), increasing gas density results in escalation of mass flow rate of the gas at a constant throat-pipe diameter ratio, and at a constant gas density, the mass flow rate decreases as diameter ratio of the throat (Beta) increases. Also, the growth of Beta at the constant volume fraction of the gas results in lower gas mass flow rate (Fig. 3(b)).

Fig. 4(a) shows the effect of Beta and oil volume fraction on mass flow rate of the oil. As depicted in Fig. 4(a), the oil flow rate increases as oil volume fraction augments, and Beta decreases. The effects of oil density on oil flow rate is similar to the effect of oil volume fraction (Fig. 4(b)).

Fig. 5 illustrates the effects of Beta, gas, and oil volume fraction on the water flow rate. As shown in Fig. 5, the reduction of Beta and augmentation of gas and oil volume fraction results in increasing water mass flow rate.

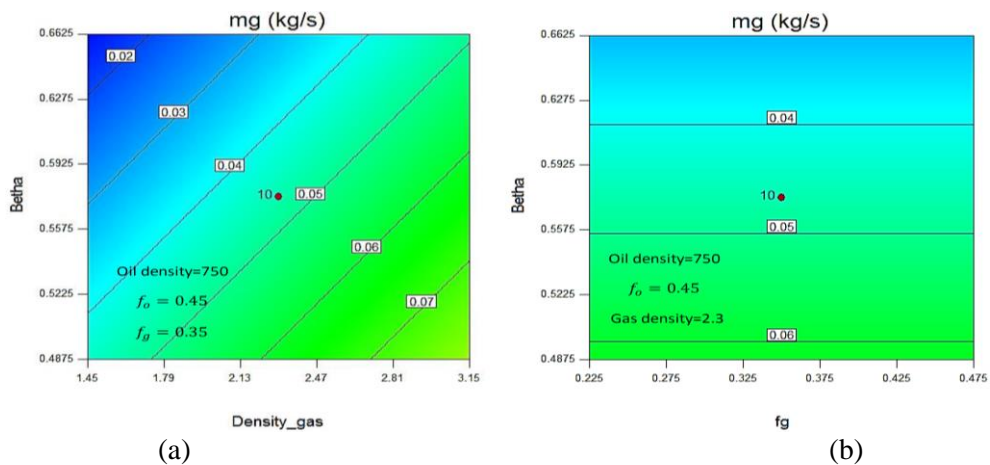


Fig. 3. The effect of throat pipe diameter ratio, gas density, and volume fraction on gas mass flow rate.

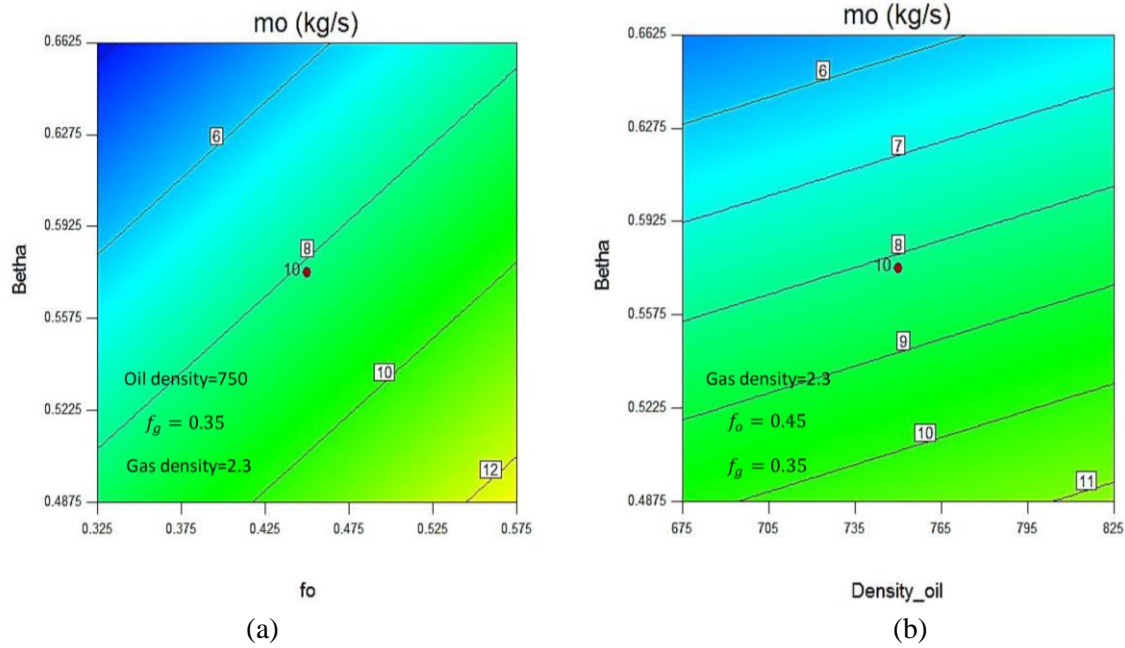


Fig. 4. The effect of throat pipe diameter ratio, oil density, and oil volume fraction on oil mass flow rate.

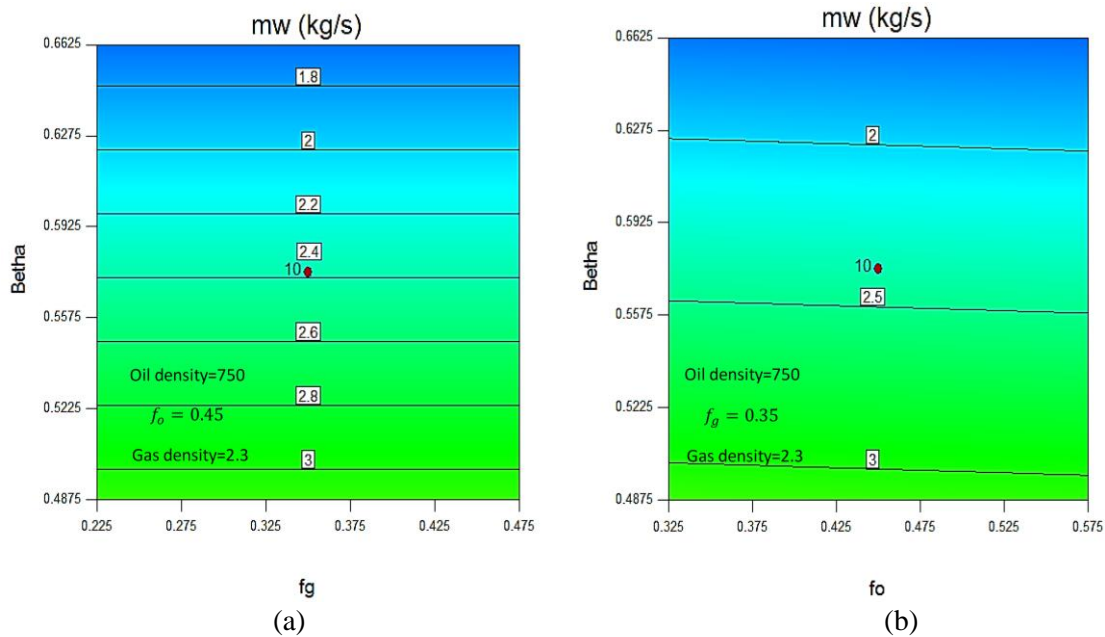
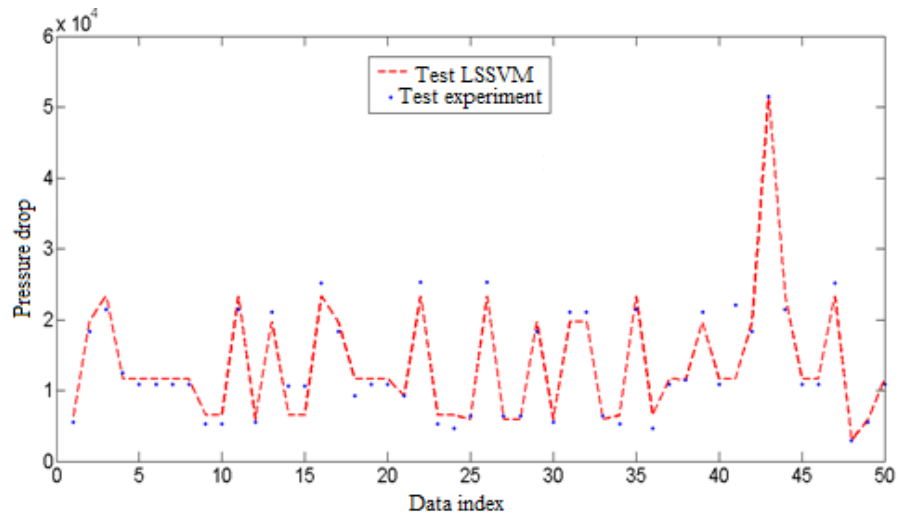


Fig. 5. The effect of throat pipe diameter ratio, gas volume fraction, and oil volume fraction on water mass flow rate.

In order to develop a more efficient model, more data must be used; therefore, the least square support vector machine is used to develop data of CFD simulation. The obtained data, reported in Table II, used as test and train data in the LSSVM algorithm.

The pressure drop, mass flow rates of gas, oil, and water are predicted with the LSSVM method. Figs. 6-9 show the result of the prediction for the mentioned parameters. The predicted data with the LSSVM method are reported in Table II (Appendix).



**Fig. 6.** The LSSVM and actual value of pressure drop during three-phase flow.

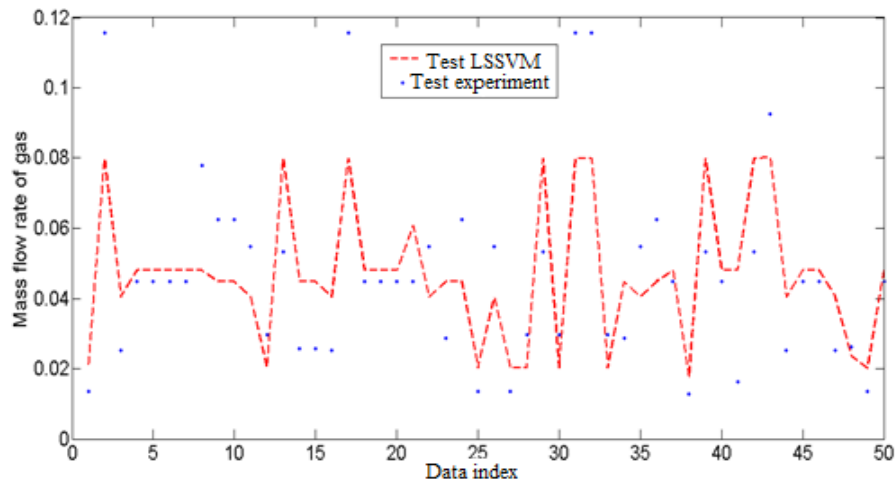


**Fig. 7.** The LSSVM and actual value of mass flow rate of gas.

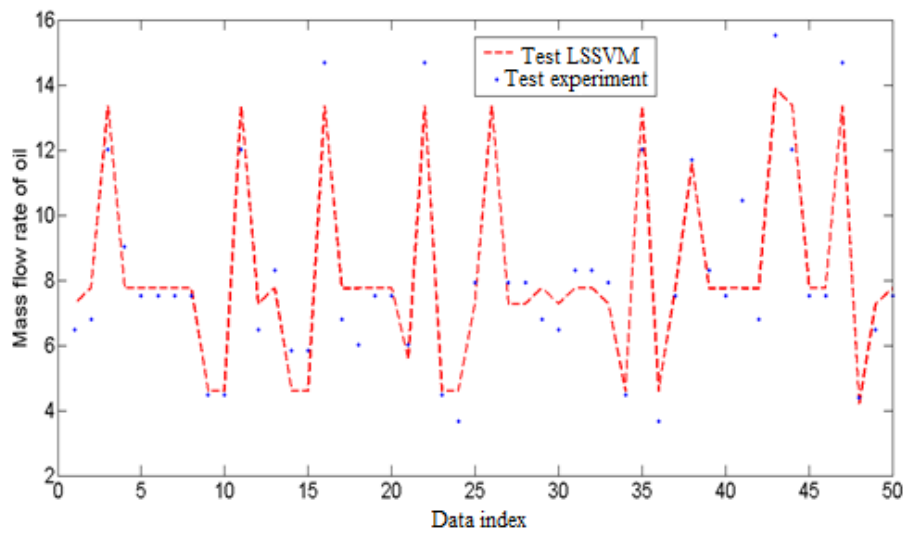


**Fig. 8.** The LSSVM and actual value of mass flow rate of oil.

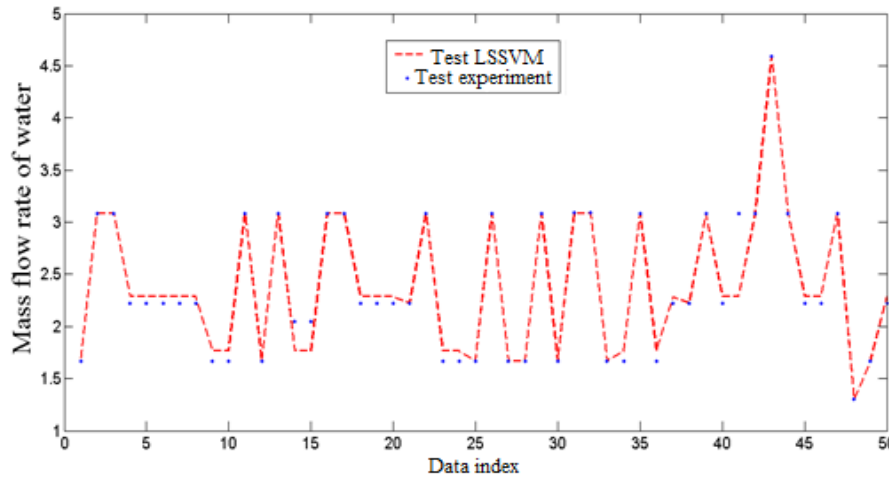


**Fig. 9.** The LSSVM and actual value of mass flow rate of water.

According to analyzes obtained using the simulator, a suitable model for a three-phase flow in Venturi can be provided. Also, this method requires a non-linear regression. There are various methods for non-linear regression between the simulation parameters such as the use of support vector machine and data mining regression. After selecting the appropriate method, it is needed to predict that sort of output data that simulation is not done for them. Because the more the number of data, the less the associated uncertainty, so a support vector machine algorithm is used to predict the desired output. However, with lots of data and MATLAB Simulink, an appropriate model is offered to predict the three-phase flow in Venturi.

In this study, the design of experiment approach is used to design CFD simulation cases. The LSSVM algorithm is used to predict pressure drop and oil, gas, and water mass flow rate based on the throat-pipe diameter ratio, the viscosity of three phases, and the volumetric ratio of three phases. Two tuning parameters of LSSVM, namely  $\gamma$  and  $\sigma^2$ , obtained as 1150954 and 0.4384, 53.9199 and 0.18163, 8.8714 and 0.14424, and 10039130.2214 and 0.74742 for pressure drop, the mass flow rate of oil, the mass flow rate of gas, and the mass flow rate of water, respectively. Gathered data set with the LSSVM algorithm containing 40 data points are reported in Table III, in the previous section. The computational models are developed with 83

data points gathered from the CFD simulation case using FLUENT and predicted cases using a support vector machine (SVM). All of the gathered data points are used for the Simulink toolbox in MATLAB software to correlate the mass flow rate of three-phase with minimum error in computations. Correlated equation of mass flow rate of three-phases is described in Eqs. (20-22). Reasonable agreement between the actual and estimated mass flow rate of gas, oil, and water are shown in Figs. 10 to 12, respectively. The obtained value of R-squared is 0.9883, 0.9886, and 0.9965 for gas mass flow rate, oil mass flow rate, and water mass flow rate, respectively. Developed models are found to have average relative errors of 5.81%, 6.31%, and 2.58% for gas, oil, and water, respectively; which are shown in Figs. 13-15. Actual and estimated values of mass flow rate of three phases are reported in Table III (Appendix).

$$\dot{m}_g = \frac{A_t K_g \sqrt{1.48 \Delta P_{tp} \rho_g}}{0.65472 X_{mod}} \quad (24)$$

$$\dot{m}_o = \frac{A_t K_g \sqrt{13.8 \Delta P_{tp} \rho_o}}{0.65472 \left( \frac{1}{X_{mod}} \right) + \left( \frac{\rho_o}{\rho_l} \right)^{1.0896}} \quad (25)$$

$$\dot{m}_w = \frac{A_t K_g \sqrt{0.55 \Delta P_{tp} \rho_w}}{0.65472 \left( \frac{1}{X_{mod}} \right) + \left( \frac{\rho_w}{\rho_l} \right)^{4.1456}} \quad (26)$$

In Eqs. 24-26,  $A_t$  is the cross-sectional area of the throat,  $K_g$  is the gas flow coefficient,  $\Delta P_{tp}$  is

the pressure drop of three-phase flow, and  $X_{mod}$  can be calculated from Eq. (27).

where  $x$  is the Lockhart-Martinelli parameter, defined as below:

$$X_{mod} = \left(\frac{1-x}{x}\right)^{0.49746} \left(\frac{K_g}{K_l}\right)^{0.31284} \sqrt{\frac{(\rho_g)^2}{\rho_w + \rho_o}} \quad (27)$$

$$x = \dot{c} \left(\frac{\varphi_g}{1-\varphi_g}\right) \left(\frac{\rho_g}{\rho_l}\right)^{0.775} \quad (28)$$

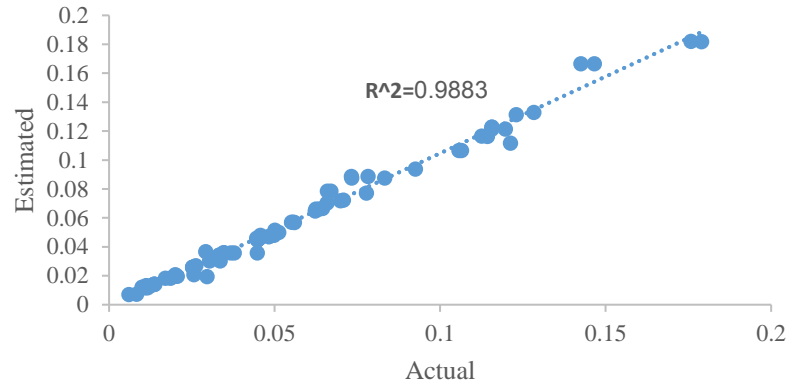


Fig. 10. Regression plot for the actual and estimated of mass flow rate of gas.

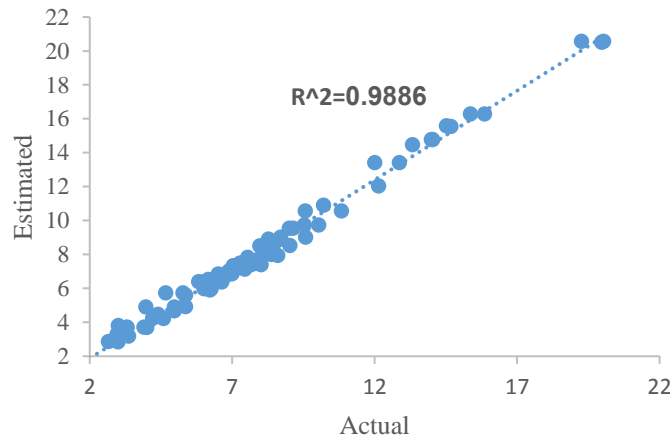


Fig. 11. Regression plot for the actual and estimated of mass flow rate.

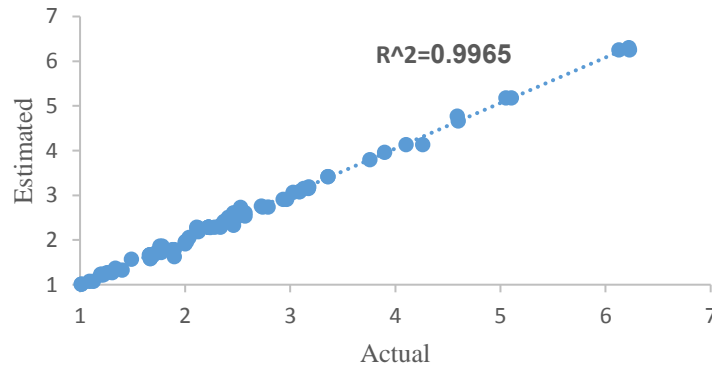
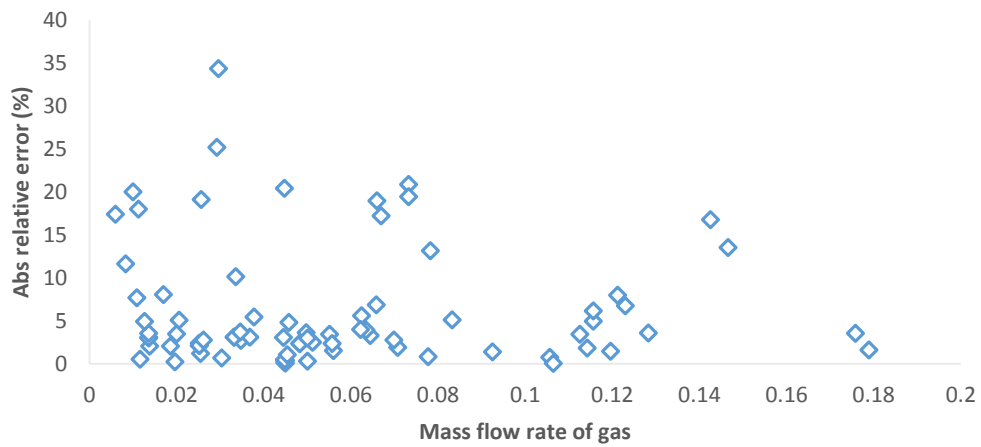
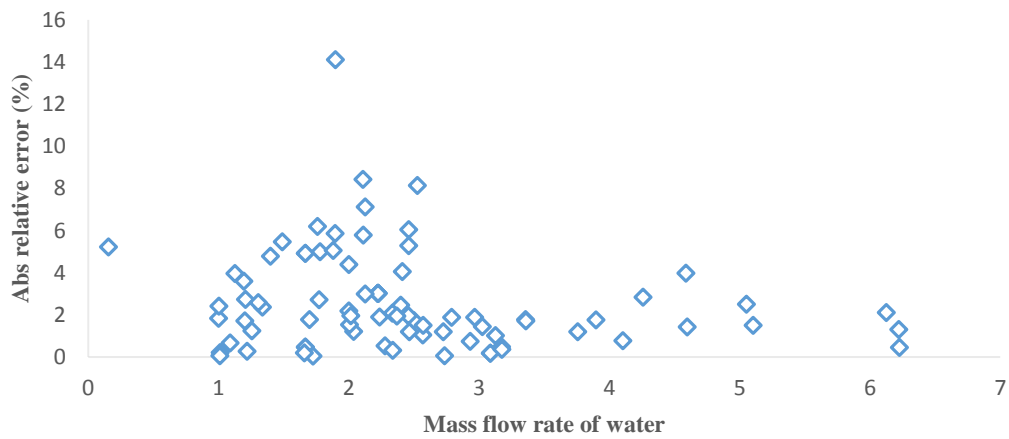


Fig. 12. Regression plot for the actual and estimated of mass flow rate of oil.



**Fig. 13.** Relative error between the actual and predicted mass flow rate of gas.



**Fig. 15.** Relative error between the actual and predicted mass flow rate of water.

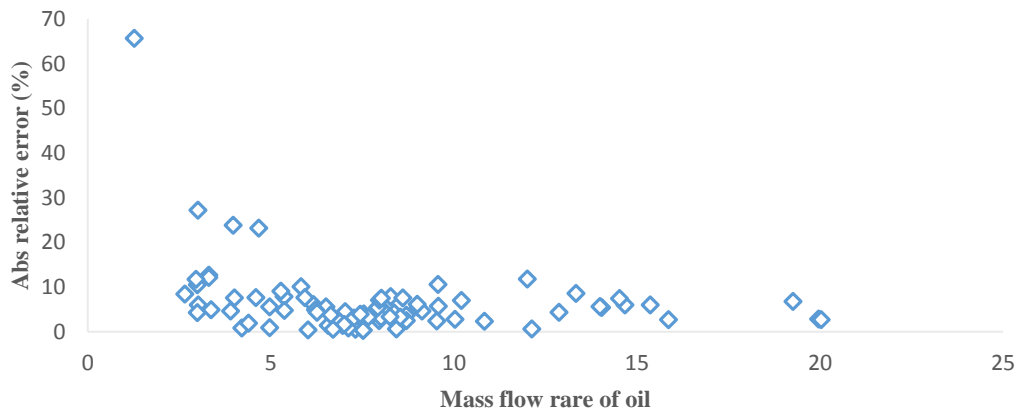


**Fig. 14.** Relative error between the actual and predicted mass flow rate of oil.

#### 4. Conclusions

In this study, a new venturi model is implemented in Simulink/Matlab for predicting the mass flow rate of gas, water, and oil. Individual data sets are simulated in ANSYS FLUENT to get hydrodynamic properties of the fluids to be used as inputs in the models. The simulations are classified with design expert® software, V10. The pressure drop, the mass flow rate of gas and oil, and the mass flow rate of water are predicted with the LSSVM method. The train and test data are obtained with validated CFD calculations to ensure the accuracy of the model. The conclusions drawn from this study are as follows:

1. The previously developed correlation for two-phase flow is complex and not capable of three-phase flow. This developed model is more accurate with minimum error.
2. The use of equations based on existing conditions is valuable to enhance the speed and accuracy in the process estimation.
3. Identifying the behavior of phases in different conditions to design and model the flow process is important and can be obtained with new developing model.
4. The data related to computational fluid dynamics software analysis are used to provide an appropriate model for the three-phase flow with the minimum error.
5. The proposed model is based on pressure difference, the ratio of the Venturi throat diameter to its inlet cross-sectional diameter, and density and volume fraction of each phase that alteration of them can significantly change the results of the simulation.
6. Two tuning parameters of LSSVM, namely  $\gamma$  and  $\sigma^2$ , are obtained as 1150954 and 0.4384, 53.9199 and 0.18163, 8.8714 and 0.14424, and 10039130.2214 and 0.74742 for the pressure drop, the mass flow rate of oil, the mass flow rate of gas, the mass flow rate of water, respectively.

#### References

- [1] H. Yeung, J. Hemp, M. Henry and M. Tombs, "Coriolis meter in liquid/liquid, gas/liquid and gas/liquid/liquid flows" , 3rd International SE Asia Hydrocarbon Flow Measurement Workshop, (2004).
- [2] G. Falcone, G. Hewitt, C. Alimonti and B. Harrison, "Multiphase flow metering: current trends and future developments", SPE annual technical conference and exhibition, Society of Petroleum Engineers, (2001).
- [3] J. P. Brill, "Modeling Multiphase Flow in Pipes", *The Way Ahead*, Vol. 6, pp. 16-17, (2010).
- [4] B. Azzopardi and A. Govan, "The modelling of venturi scrubbers", Filtech conference, (1983).
- [5] R. A. Pulley, "Modelling the performance of venturi scrubbers." *Chemical Engineering Journal*, Vol. 67, No. 1, pp. 9-18, (1997).
- [6] J. Murdock, "Two-phase flow measurement with orifices", *Journal of basic engineering*, Vol. 84, No. 4, pp. 419-432, (1962).
- [7] Z. Lin, "Two-phase flow measurements with sharp-edged orifices", *International Journal of Multiphase Flow*, Vol. 8, No. 6, pp. 683-693, (1982).
- [8] R. Smith and J. Leang, "Evaluations of correlations for two-phase, flowmeters three current-one new", *Journal of Engineering for Power*, Vol. 97, No. 4, pp. 589-593, (1975).
- [9] R. De Leeuw, "*Liquid correction of Venturi meter readings in wet gas flow*", North Sea Flow Measurement Workshop, p. 335 (1997).
- [10] D. Chisholm, "Two-phase flow in heat exchangers and pipelines.", *Heat transfer engineering*, Vol. 6, No. 2, pp. 48-57, (1985).
- [11] R. N. Steven, "Wet gas metering with a horizontally mounted Venturi meter", *Flow measurement and Instrumentation*, Vol. 12, No. 5-6, pp. 361-372, (2002).
- [12] A. Tukimin, M. Zuber and K. Ahmad, "CFD analysis of flow through Venturi tube and its discharge coefficient", *Materials Science and Engineering, IOP Publishing*, Vol. 152, No. 1, pp. 012062, (2016).
- [13] J. L. G. Oliveira, J. C. Passos, R. Verschaeren and C. van der Geld, "Mass flow rate measurements in gas-liquid flows by means of a venturi or orifice plate coupled to a void fraction sensor", *Experimental Thermal and Fluid Science*, Vol. 33, No. 2, pp. 253-260, (2009).
- [14] D. He and B. Bai, "A new correlation for wet gas flow rate measurement with Venturi

- meter based on two-phase mass flow coefficient", *Measurement*, Vol. 58, pp. 61-67, (2014).
- [15] L. Xu, J. Xu, F. Dong and T. Zhang, "On fluctuation of the dynamic differential pressure signal of Venturi meter for wet gas metering", *Flow measurement and instrumentation*, Vol. 14, No. 4-5, pp. 211-217, (2003).
- [16] L. F. Moura and C. Marvillet, "Measurement of two-phase mass flow rate and quality using venturi and void fraction meters", *American Society of Mechanical Engineers, Fluids Engineering Division (Publication) FED*, (1997).
- [17] B. Gupta, A. Nayak, T. Kandar and S. Nair, "Investigation of air–water two phase flow through a venturi", *Experimental Thermal and Fluid Science*, Vol. 70, pp. 148-154, (2016).
- [18] E. Stenmark, "On multiphase flow models in ANSYS CFD software, Department of Applied Mechanics Division of Fluid Dynamics", Chalmers university of technology. Göteborg, Sweden, Vol. 75, (2013).
- [19] N. Kharoua, L. Khezzar and H. Saadawi, "CFD modelling of a horizontal three-phase separator: a population balance approach", *American Journal of Fluid Dynamics*, Vol. 3, No. 4, pp. 101-118, (2013).
- [20] F.S. Silvaeo, P. Andreussi and P. Di Marco, "Total mass flowrate measurement in multiphase flow by means of a venturi meter", *Multiphase Production*, pp. 145-155, (1991).
- [21] D. Collins and M. Gacesa, "Measurement of Steam Quality in Two-Phase Upflow with Venturimeters", *Fluids Engineering, Heat Transfer and Lubrication Conference*, Vol. 93, No. 1, pp. 11-20, (1971).
- [22] Y. Ling, A. Haselbacher, S. Balachandar, "A numerical source of small-scale number-density fluctuations in Eulerian–Lagrangian simulations of multiphase flows", *Journal of Computational Physics*, Vol. 229, No. 5, pp. 1828-1851, (2010).
- [23] H. Zhang, S. Lu and G. Yu, "An investigation of two-phase flow measurement with orifices for low-quality mixtures", *International journal of multiphase flow*, Vol. 18, No. 1, pp. 149-155, (1992).
- [24] Z. Meng, Z. Huang, B. Wang, H. Ji, H. Li and Y. Yan, "Air–water two-phase flow measurement using a Venturi meter and an electrical resistance tomography sensor", *Flow Measurement and Instrumentation*, Vol. 21, pp. 268-276, (2010).
- [25] A. Fiebach, E. Schmeier, S. Knotek and S. Schmelter, "Numerical simulation of multiphase flow in a vertically mounted Venturi flow meter", pp. 26-29, (2016).
- [26] T. Frank, "Advances in computational fluid dynamics (CFD) of 3-dimensional gas-liquid multiphase flows", NAFEMS Seminar: Simulation of Complex Flows (CFD)–Applications and Trends, Wiesbaden, Germany, Citeseer, pp. 1-18, (2005).
- [27] S. Akbari, and S. H. Hashemabadi. "Temperature and pressure effects of drilling fluid on cutting transport using CFD simulations", *Asia-Pacific Journal of Chemical Engineering*, Vol. 12, No. 6, pp. 980-992, (2017).
- [28] K. Mohammadzadeh, S. H. Hashemabadi and S. Akbari. "CFD simulation of viscosity modifier effect on cutting transport by oil based drilling fluid in wellbore", *Journal of Natural Gas Science and Engineering*, Vol. 29, pp. 355-364, (2016).
- [29] A. Taghizadeh, S. H. Hashemabadi, E. Yazdani and S. Akbari, "Numerical analysis of restitution coefficient, rotational speed and particle size effects on the hydrodynamics of particles in a rotating drum", *Granular Matter*, Vol. 20, No. 3, p. 56, (2018).
- [30] M. Manninen, V. Taivassalo and S. Kallio, "On the mixture model for multiphase flow", pp. 3-67, (1996).
- [31] B. E. Launder and D. B. Spalding, "The numerical computation of turbulent flows", *Computer Methods in Applied Mechanics & Engng.* Vol. 3, No. 2, pp. 269-289 (1974).
- [32] H. K. Versteeg and W. Malalasekera, *An introduction to computational fluid dynamics*, 2<sup>nd</sup> ed., Pearson Education, England, (2007).
- [33] C. Sanghani and D. Jayani, "Optimization of Venturimeter Geometry for Minimum Pressure Drop using CFD Analysis", *Recent*

*Trends in Fluid Mechanics*, Vol. 3, pp. 31-35, (2016).

[34] H. A. P. Perez, J. E. Lopez, N. R. Ratkovich, M. d. M. F. Figueiredo, R. D. M. de Carvalho and J. S. Slongo, "Three-Dimensional Simulations of Liquid-Gas Flows at the NEAT-PETROBRAS Test Loop for Calibration of an Ultrasonic Multiphase Flow Meter", *IV Journeys in Multiphase Flows* (2015).

[35] V. Michele and D. C. Hempel, "Liquid flow and phase holdup measurement and CFD modeling for two-and three-phase bubble columns", *Chemical engineering science*, Vol. 57, No. 11, pp. 1899-1908, (2002).

[36] K. Ekambara, R. Sanders, K. Nandakumar and J. Masliyah, "CFD simulation of bubbly two-phase flow in horizontal pipes", *Chemical Engineering Journal*, Vol. 144, No. 2, pp. 277-288, (2008).

[37] A. Baghban, P. Abbasi, P. Rostami, M. Bahadori, Z. Ahmad, T. Kashiwao and A. Bahadori, "Estimation of oil and gas properties in petroleum production and processing operations using rigorous model", *Petroleum Science and Technology*, Vol. 34, No. 13, pp. 1129-1136, (2016).

[38] J. A. Suykens, T. Van Gestel and J. De Brabanter, *Least squares support vector machines*, World Scientific, (2002).

[39] A. E. Hoerl and R. W. Kennard, "Ridge regression: Biased estimation for nonorthogonal problems", *Technometrics*, Vol. 12, No. 1, pp. 55-67, (1970).

**Appendix**

**Table I.** The collected data for classification of numerical simulation .

Run	$\beta$	Oil density(Kg/m <sup>3</sup> )	Gas density(Kg/m <sup>3</sup> )	$\phi_o$	$\phi_g$
1	0.6625	675	1.45	0.575	0.225
2	0.4875	675	3.15	0.325	0.475
3	0.4875	675	1.45	0.575	0.225
4	0.575	900	2.3	0.45	0.35
5	0.575	750	2.3	0.45	0.35
6	0.575	750	4	0.45	0.35
7	0.6625	825	3.15	0.325	0.475
8	0.4875	675	3.15	0.575	0.225
9	0.6625	675	3.15	0.575	0.225
10	0.4875	825	1.45	0.325	0.475
11	0.6625	675	1.45	0.325	0.475
12	0.4875	825	1.45	0.575	0.225
13	0.4875	675	3.15	0.325	0.475
14	0.575	600	2.3	0.45	0.35
15	0.575	750	2.3	0.45	0.35
16	0.575	750	2.3	0.2	0.6
17	0.4875	825	3.15	0.58	0.23
18	0.6625	825	1.45	0.325	0.475
19	0.6625	675	3.15	0.325	0.475
20	0.6625	825	1.45	0.575	0.225
21	0.4875	825	3.15	0.575	0.225
22	0.6625	825	1.45	0.575	0.225
23	0.6625	825	3.15	0.575	0.225
24	0.4875	675	1.45	0.325	0.475
25	0.6625	675	3.15	0.575	0.225
26	0.4875	825	3.15	0.325	0.475
27	0.6625	825	3.15	0.575	0.225
28	0.6625	825	1.45	0.325	0.475
29	0.4875	675	3.15	0.575	0.225
30	0.6625	675	3.15	0.325	0.475
31	0.575	750	2.3	0.45	0.35
32	0.575	750	2.3	0.7	0.1
33	0.4875	825	1.45	0.325	0.475
34	0.575	750	2.3	0.45	0.35
35	0.575	750	0.6	0.45	0.35
36	0.4875	675	1.45	0.325	0.475
37	0.4	750	2.3	0.45	0.35
38	0.4875	675	1.45	0.575	0.225
39	0.575	750	2.3	0.45	0.35
40	0.4875	825	1.45	0.575	0.225
41	0.75	750	2.3	0.45	0.35
42	0.6625	675	1.45	0.575	0.225
43	0.575	750	2.3	0.45	0.35

**Table II.** The predicted data of LSSVM method.

Run	$\beta$	Oil density(Kg/m <sup>3</sup> )	Gas density(Kg/m <sup>3</sup> )	$\phi_o$	$\phi_g$
44	0.3875	837.5	3.0125	0.575	0.225
45	0.5250	725.0	2.0250	0.450	0.350
46	0.5250	725.0	0.0500	0.450	0.350
47	0.3875	612.5	1.0375	0.575	0.225
48	0.6625	837.5	1.0375	0.325	0.475
49	0.5250	500.0	2.0250	0.450	0.350
50	0.5250	725.0	4.0000	0.450	0.350
51	0.6625	612.5	1.0375	0.575	0.225
52	0.2500	725.0	2.0250	0.450	0.350
53	0.3875	837.5	3.0125	0.575	0.225
54	0.3875	837.5	3.0125	0.325	0.475
55	0.6625	837.5	3.0125	0.325	0.475
56	0.6625	837.5	1.0375	0.575	0.225
57	0.6625	837.5	3.0125	0.575	0.225
58	0.6625	612.5	1.0375	0.325	0.475
59	0.5250	725.0	2.0250	0.450	0.350
60	0.6625	612.5	3.0125	0.575	0.225
61	0.3875	837.5	1.0375	0.575	0.225
62	0.5250	725.0	2.0250	0.700	0.100
63	0.3875	612.5	1.0375	0.575	0.225
64	0.3875	612.5	1.0375	0.325	0.475
65	0.3875	612.5	3.0125	0.325	0.475
66	0.6625	612.5	3.0125	0.325	0.475
67	0.8000	725.0	2.0250	0.450	0.350
68	0.6625	612.5	3.0125	0.325	0.475
69	0.6625	837.5	3.0125	0.325	0.475
70	0.6625	612.5	1.0375	0.325	0.475
71	0.3875	837.5	1.0375	0.575	0.225
72	0.3875	837.5	1.0375	0.325	0.475
73	0.3875	612.5	3.0125	0.325	0.475
74	0.3875	612.5	1.0375	0.325	0.475
75	0.5250	950.0	2.0250	0.450	0.350
76	0.6625	837.5	3.0125	0.575	0.225
77	0.6625	612.5	1.0375	0.575	0.225
78	0.3875	837.5	3.0125	0.325	0.475
79	0.3875	837.5	1.0375	0.325	0.475
80	0.5250	725.0	2.0250	0.200	0.600
81	0.6625	837.5	1.0375	0.325	0.475
82	0.6625	612.5	3.0125	0.575	0.225
83	0.6625	837.5	1.0375	0.575	0.225

**Table III.** Actual and estimated values of mass flow rate of three phases.

Run	Actual $M_g$	Estimated $M_g$	Actual $M_o$	Estimated $M_o$	Actual $M_w$	Estimated $M_w$
1	0.0138	0.0141	4.199	4.234	1.256	1.272
2	0.1196	0.1213	10.826	10.571	3.086	3.080
3	0.0255	0.0258	7.952	7.753	2.456	2.329
4	0.0449	0.0451	9.022	8.528	2.789	2.758
5	0.0449	0.0450	7.918	7.489	2.278	2.290
6	0.0559	0.0568	10.190	10.915	3.025	3.069
7	0.0644	0.0665	6.159	6.533	2.036	2.061
8	0.0347	0.0357	12.867	13.423	3.356	3.414
9	0.0205	0.0195	7.029	7.343	1.759	1.423
10	0.0732	0.0885	6.474	6.860	2.109	2.287
11	0.0708	0.0721	5.987	4.936	1.896	1.629

12	0.0252	0.0257	8.657	9.020	2.965	2.910
13	0.1156	0.1213	9.689	10.571	3.085	3.080
14	0.0448	0.0449	5.812	6.403	1.772	1.724
15	0.0448	0.0450	7.812	7.489	2.223	2.290
16	0.1283	0.1329	6.218	5.905	2.001	1.956
17	0.0447	0.0356	5.460	5.269	1.990	1.925
18	0.0497	0.0479	3.298	3.716	1.205	1.238
19	0.0624	0.0659	4.663	5.743	1.666	1.674
20	0.0136	0.0140	3.968	4.914	1.667	1.585
21	0.0400	0.0356	14.670	15.554	4.600	4.663
22	0.0136	0.0140	4.958	4.914	1.667	1.585
23	0.0295	0.0194	8.425	8.477	2.568	2.542
24	0.0732	0.0874	6.012	5.985	2.005	1.975
25	0.0195	0.0195	7.302	7.343	1.779	1.868
26	0.1156	0.1228	12.129	12.049	3.756	3.803
27	0.0457	0.0479	8.125	8.477	2.498	2.542
28	0.0377	0.0357	3.897	3.7160	1.195	1.238
29	0.0634	0.0659	12.001	13.423	3.358	3.416
30	0.0448	0.0450	5.265	5.745	1.666	1.674
31	0.0082	0.0073	7.518	7.489	2.223	2.290
32	0.0782	0.0885	10.025	9.743	2.526	2.732
33	0.0448	0.0450	6.958	6.860	2.335	2.287
34	0.0292	0.0365	7.518	7.489	2.223	2.290
35	0.0832	0.0874	3.002	3.820	1.396	1.331
36	0.0925	0.0937	6.259	5.985	2.018	1.975
37	0.0252	0.0258	14.514	15.598	4.588	4.771
38	0.0448	0.0450	8.006	7.753	2.336	2.329
39	0.0252	0.0257	7.918	7.489	2.223	2.290
40	0.0261	0.0268	9.568	9.021	2.932	2.910
41	0.0136	0.0141	4.389	4.472	1.336	1.368
42	0.0448	0.0450	4.587	4.234	1.305	1.272
43	0.0482	0.0471	7.265	7.485	2.223	2.290
44	0.0551	0.0570	19.258	20.570	6.226	6.254
45	0.0100	0.0120	8.698	8.914	2.734	2.737
46	0.0332	0.0342	1.265	0.434	0.156	0.164
47	0.0454	0.0459	7.958	8.522	2.569	2.608
48	0.0622	0.0647	3.012	3.194	1.125	1.081
49	0.0777	0.0771	7.536	7.836	2.000	1.912
50	0.0112	0.0132	13.325	14.475	3.898	3.964
51	0.1229	0.1312	2.987	3.301	1.012	1.010
52	0.0482	0.0471	19.958	20.526	6.221	6.302
53	0.1425	0.1664	20.025	20.570	6.125	6.251
54	0.0698	0.0717	15.359	16.287	5.102	5.178
55	0.0108	0.0116	6.874	7.024	2.111	2.233
56	0.0169	0.0183	3.297	3.699	1.219	1.223
57	0.0500	0.0502	8.365	8.013	2.465	2.436
58	0.0556	0.0570	2.647	2.870	1.008	0.983
59	0.0256	0.0207	8.264	8.914	2.789	2.737
60	0.0335	0.0301	7.108	7.171	1.698	1.668
61	0.0059	0.0070	9.12	9.550	3.125	3.157
62	0.0332	0.0342	8.525	8.804	2.398	2.457
63	0.1125	0.1164	8.247	8.524	2.459	2.608
64	0.1758	0.1820	6.562	6.656	2.236	2.279
65	0.0659	0.0785	14.027	14.791	4.258	4.127
66	0.0346	0.0359	5.925	6.379	1.895	1.784
67	0.0669	0.0785	5.362	5.618	1.725	1.725
68	0.0658	0.0703	6.631	6.379	1.879	1.784
69	0.0512	0.0499	7.002	6.885	2.125	2.189
70	0.0303	0.0301	2.986	2.857	1.002	0.978

71	0.1056	0.1064	8.995	9.550	3.172	3.157
72	0.1789	0.1818	7.659	7.405	2.458	2.506
73	0.1142	0.1163	13.980	14.777	4.102	4.133
74	0.0500	0.0515	6.689	6.651	2.125	2.277
75	0.0185	0.0181	9.521	9.750	3.175	3.187
76	0.0126	0.0132	8.595	7.945	2.369	2.415
77	0.1465	0.1664	2.954	3.301	1.006	1.010
78	0.1064	0.1065	15.850	16.287	5.052	5.178
79	0.1212	0.1115	8.011	7.407	2.409	2.507
80	0.0445	0.0459	4.962	4.685	1.489	1.571
81	0.0199	0.0206	3.361	3.194	1.088	1.081
82	0.0116	0.0116	7.439	7.147	1.659	1.663
83	0.0449	0.0450	4.002	3.699	1.202	1.223

**How to cite this paper:**

*Omid Khayat and Hossein Afarideh, “ Numerical modeling of three-phase flow through a Venturi meter using the LSSVM algorithm”, Journal of Computational and Applied Research in Mechanical Engineering, Vol. 10, No. 1, pp. 153-170, (2020).*

**DOI:** 10.22061/jcarme.2019.3637.1423

**URL:** [http://jcarme.sru.ac.ir/?\\_action=showPDF&article=1046](http://jcarme.sru.ac.ir/?_action=showPDF&article=1046)

